Self-Assembly of Supramolecules Consisting of Octyl Gallate Hydrogen Bonded to Polyisoprene-*block*-poly(vinylpyridine) Diblock Copolymers

Sasa Bondzic, Joost de Wit, Evgeny Polushkin, Arend Jan Schouten, and Gerrit ten Brinke*

Laboratory of Polymer Chemistry, Materials Science Centre, University of Groningen, Nijenborgh 4, 9747AG Groningen, The Netherlands

Janne Ruokolainen and Olli Ikkala*

Department of Engineering Physics and Mathematics, Center for New Materials, Helsinki University of Technology, P.O. Box 2200, FIN-02015 HUT, Espoo, Finland

Igor Dolbnya and Wim Bras

Dubble CRG/ESRF, Netherlands Organization for Scientific Research (NWO), c/o BP 220, F-38043, Grenoble Cedex 9, France

Received June 2, 2004; Revised Manuscript Received August 13, 2004

ABSTRACT: Synchrotron radiation was used to investigate the self-assembly in two comb-shaped supramolecules systems consisting of octyl gallate (OG), i.e., 1-octyl-3,4,5-trihydroxybenzoate, hydrogen bonded to the pyridine groups of polyisoprene-*block*-poly(vinylpyridine) diblock copolymers. In the case of the 1,2-polyisoprene-*block*-poly(4-vinylpyridine)$(OG)_x$ system, self-assembly was only observed for $x \geq 0.5$, where x denotes the number of OG molecules per pyridine group. For $x = 0.5$, 0.75, 1.0, and 1.2 the system self-assembled in the form of hexagonally ordered cylinders of P4VP(OG) throughout the entire temperature range of 25−200 °C investigated. For the 1,4-polyisoprene-*block*-poly(2-vinylpyridine)$(OG)_x$ system, on the other hand, a considerably more complex phase behavior was found, including the formation of cubic, hexagonally ordered cylinders and lamellar morphologies. In this case several order−order transitions were observed as a function of temperature, including a lamellar to lamellar transition involving a collapse of the layer thickness. The absence of hydrogen bonding between the octyl gallate molecules and the pyridine groups at elevated temperatures is argued to be a key factor for many of the phenomena observed.

Introduction

Self-assembly of block copolymer-based systems has attracted considerable attention during the past decades.[1−6] It is of great interest in the area of nanotechnology which largely depends on the ability to arrange functional materials at the nanoscale.[6,7] Block copolymers self-assemble in a variety of ordered structures depending on several parameters such as the number of copolymer blocks, their volume fraction, chain flexibility, architecture, and the extent of repulsion between the chemically connected blocks. The ordered structures include the classical body-centered-cubic (bcc), hexagonal cylinder, and lamellar phases as well as more complex structures. These block copolymer morphologies have a characteristic length scale which is usually in the 10−100 nm range.

Recently, different concepts to achieve self-assembled polymeric structures at a smaller length scale (typically 3−5 nm) have been presented. The essential ingredient is the presence of a comb-shaped architecture due to complexation between polymers and amphiphilic molecules by physical interactions, e.g., ionic,[8,9] hydrogen bonding,[10−13] or metal coordination.[14,15] When the side groups are mesogenic, supramolecular side-chain liquid crystalline polymers are formed.[16−21] In this paper, we will concentrate on comb-shaped supramolecules obtained via hydrogen bonding of nonmesogenic amphiphiles. Hydrogen-bonding interactions are usually considerably weaker than ionic interactions or metal coordination, and the thermal reversibility of the hydrogen bonds is an important additional asset which can allow new functions. One of the simplest examples involves the hydrogen bonding between pentadecylphenol (PDP) and poly(4-vinylpyridine) (P4VP). Here, the competition between attraction and repulsion leads to a self-assembled lamellar morphology below ca. 65 °C.[22] Combining this ordering with that of diblock copolymers, e.g., polystyrene-*block*-poly(4-vinylpyridine) (PS-*b*-P4VP), gives rise to a variety of structure-*within*-structure morphologies.[11,13] Selecting suitable block lengths, a lamellar-*within*-cylinder structure has been obtained with hexagonally ordered cylinders containing self-assembled lamellae of P4VP(PDP) inside a glassy PS matrix. Hollow cylinders with P4VP brushes at the interior wall are formed by simply dissolving the PDP molecules away.[23] This "hairy tube" concept opens possibilities for preparation of controllable mesoporous functional membranes. The brushes themselves can be selected for a specific surface activity of the pore walls, but more clever functions may be envisioned such as switching transport properties.[10,11]

These materials are excellent candidates for preparing functional nanostructured materials in a bottom-up procedure. However, the realization of this potential depends to a large extent on our ability to control the orientation and lateral ordering of the nanoscopic domains. Therefore, many groups are currently involved in developing methodologies to achieve well-ordered macroscopically aligned systems. Several routes employing different external fields have been explored, e.g.,

10.1021/ma048913r CCC: $27.50
Published on Web 11/18/2004

Table 1. Samples Investigated

designation	block copolymer	M_n(PI)/M_n(PVP)g/mol	$x = n$(OG)/n(VP)	PVP(OG)$_x$% w/w
PI-*b*-P4VP	1,2-PIp-*b*-P4VP	12500/1000	0.00	7.4
PI-*b*-P4VP(OG)$_{0.25}$	1,2-PIp-*b*-P4VP	12500/1000	0.25	11.8
PI-*b*-P4VP(OG)$_{0.50}$	1,2-PIp-*b*-P4VP	12500/1000	0.50	15.8
PI-*b*-P4VP(OG)$_{0.75}$	1,2-PIp-*b*-P4VP	12500/1000	0.75	19.4
PI-*b*-P4VP(OG)$_{1.00}$	1,2-PIp-*b*-P4VP	12500/1000	1.00	22.8
PI-*b*-P4VP(OG)$_{1.20}$	1,2-PIp-*b*-P4VP	12500/1000	1.20	25.2
PI-*b*-P2VP	1,4-PIp-*b*-P2VP	30000/2800	0.00	8.5
PI-*b*-P2VP(OG)$_{0.25}$	1,4-PIp-*b*-P2VP	30000/2800	0.25	13.5
PI-*b*-P2VP(OG)$_{0.50}$	1,4-PIp-*b*-P2VP	30000/2800	0.50	17.9
PI-*b*-P2VP(OG)$_{0.75}$	1,4-PIp-*b*-P2VP	30000/2800	0.75	21.9
PI-*b*-P2VP(OG)$_{1.00}$	1,4-PIp-*b*-P2VP	30000/2800	1.00	25.6
PI-*b*-P2VP(OG)$_{1.20}$	1,4-PIp-*b*-P2VP	30000/2800	1.20	28.3

large-amplitude oscillatory shear, electric fields, temperature gradients, graphoepitaxy, chemically patterned substrates, controlled interfacial interactions, and solvent control. The achievements in this field have been reviewed in a recent paper,[6] where most of the pertinent publications can be found. In recent years we demonstrated that the hierarchically structured materials produced according to the comb-shaped supramolecules concept can also be macroscopically aligned by oscillatory shear.[24−27] Very recently two papers appeared devoted to solvent controlled perpendicular alignment of cylinders on top of a substrate.[28,29] The paper of Stamm and co-workers[29] is of particular interest, since their study involves the comb-shaped supramolecules concept using 2-(4′-hydroxybenzeneazo)benzoic acid hydrogen bonded to the vinylpyridine block of polystyrene-*block*-poly(4-vinylpyridine) diblock copolymers.

As mentioned above, one of the assets of our comb-shaped supramolecule approach is the simplicity of making functional nanoporous films. For a given block copolymer, the size of the nanopores can be easily tuned by for example the block lengths or the amount of amphiphiles used. However, for certain applications it is necessary to have membranes with a pore size that can still be fine-tuned after their formation. This can in principle be realized using an elastic matrix, such as cross-linked polyisoprene, were the diameter of the pores can simply be increased in a continuous fashion using biaxial strain.

In this paper we describe the first steps of our efforts toward the preparation of these type of membranes by reporting the phase behavior of new comblike supramolecules systems based on polyisoprene-*block*-poly(vinylpyridine) diblock copolymers and octyl gallate amphiphiles.

Experimental Section

Materials. 1,2-Polyisoprene-*block*-poly(4-vinylpyridine) (PI-*b*-P4VP) diblock copolymer of molecular weight 12500/1000 g/mol, respectively (polydispersity 1.09), and 1,4-polyisoprene-*block*-poly(2-vinylpyridine) (PI-*b*-P2VP) diblock copolymer of molecular weight 30000/2800 g/mol, respectively (polydispersity 1.06, expected microstructure: *cis*-1,4 addition: 81 mol %; *trans*-1,4 addition: 15 mol %; 3,4 addition: 4 mol %), were obtained from Polymer Source, and they were used as received. Octyl gallate (OG), obtained from Sigma-Aldrich, was recrystallized from an ethanol/chloroform (9:1 volume ratio) azeotropic mixture prior to use. Scheme 1 shows the chemical structures of these materials.

Sample Preparation. Comb-shaped block copolymeric supramolecules were prepared from a chloroform solution. The concentration of polymer in the solvent was kept low (less than 2 wt %) to ensure homogeneous complex formation. After solvent evaporation, samples were put into a vacuum oven at 40 °C for 24 h to remove residual solvent. The systems

Scheme 1. Top to Bottom: 1,2-Polyisoprene-*b*-poly(4-vinylpyridine), 1,4-Polyisoprene-*b*-poly(2-vinylpyridine), and Octyl Gallate

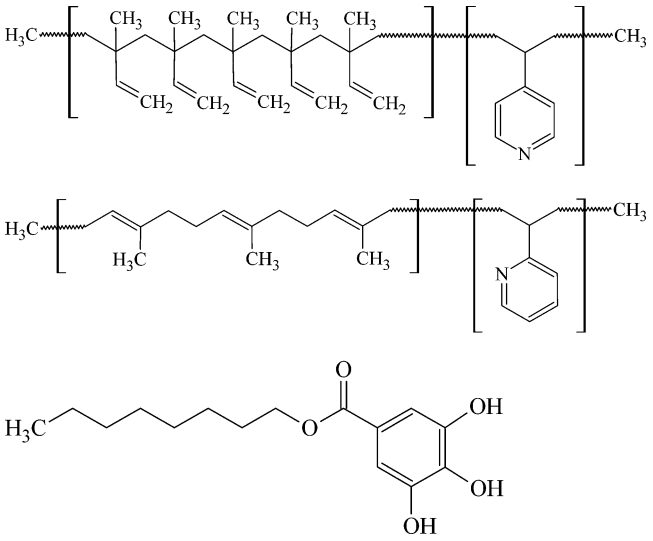

investigated are denoted as PI-*b*-P4VP(OG)$_x$ and PI-*b*-P2VP(OG)$_x$, where x is the nominal ratio between the number of octyl gallate molecules and pyridine groups (see Table 1).

SAXS Experiments. SAXS measurements were performed at the European Synchrotron Radiation Facility (ESRF, beamline BM26 "DUBBLE") in Grenoble. Experiments were performed using X-rays of wavelength $\lambda = 0.124$ nm ($E = 10$ keV). The size of the primary beam at the sample position was approximately 0.2×0.2 mm^2. The scattering vector $q = (4\pi/\lambda)\sin(\theta/2)$, where θ is the scattering angle. The sample−detector distance was 8.0 m. A two-dimensional detector was used to measure a quarter of the SAXS patterns in the q range of 0.06−0.80 nm^{-1}. The experiments were performed using a Linkam hot stage on heating with 10 °C/min and cooling with 10 or 30 °C/min in the range 25−200/220 °C depending on sample. Data were collected during 30 s for each frame.

IR Spectroscopy. Infrared spectra were obtained using Bruker IFS88 FT-IR spectrophotometer, equipped with a Specac Golden Heated Top-plate Diamond ATR. The measurements were carried out in the temperature range 30−200 °C, with a step of 10 °C.

TEM. Bulk samples of PI-*block*-P2VP(OG) for TEM characterization were embedded in epoxy and cured at 60 °C overnight. Ultrathin sections (approximately 70 nm) were cryomicrotomed from the embedded specimen using a Leica Ultracut UCT-ultramicrotome and a Diatome diamond knife at −100 °C. Dry sections were picked up onto lacey carbon film coated copper grids, and to enhance contrast, the microtomed sections were stained for 2−3 h in vapors of iodine crystals. Bright-field TEM was performed on JEOL-1200EX transmission electron microscope operating at an accelerating voltage of 60 kV.

Results and Discussion

An important part of our work during the past decade has been based on polystyrene-*block*-poly(4-vinylpyridine) (PS-*b*-P4VP) block copolymers using pentadecylphenol (PDP) or nonadecylphenol (NPD) as hydrogen-bonded side chains. Varying the relative block lengths of PS-*b*-P4VP, all classical structures were observed.[13] Most interestingly, an additional small length scale lamellar ordering occurs inside the P4VP(PDP) or P4VP(NDP) domains, thus leading to so-called hierarchically ordered materials.[11−13,20] Apart from this hierarchical ordering, the presence of hydrogen-bonded amphiphiles allows to prepare nanoporous materials by simply dissolving the amphiphiles away after they have served their role in the self-assembly process. One example, that is of direct relevance to the present investigation, concerns the hexagonally ordered structure of P4VP(PDP) cylinders in a PS matrix obtained for suitably chosen block lengths. After dissolving the hydrogen-bonded side chains in a proper solvent such as ethanol, partly empty cylinders inside a PS-matrix are obtained with P4VP chains protruding from the cylinder walls.[23] The essential difference between this and other concepts is that here the pore walls will be automatically functionalized by a dense polymer brush. In the above example the matrix consists of glassy PS, but for many applications it is advantageous to have a matrix that behaves elastically at room temperature, such as cross-linked polyisoprene, where the pore size can then be tuned further by applying two-directional strain. To this end, for the present study we selected polyisoprene-*block*-poly(4-vinylpyridine) (PI-*b*-P4VP) and polyisoprene-*block*-poly(2-vinylpyridine) (PI-*b*-P2VP) copolymers as the block copolymer component. It turned out that for both diblock copolymer systems the choice of PDP as the hydrogen-bonding side chain does not result in the desired microphase separation. Apparently, the solubility of PDP in PI, as confirmed with optical microscopy, improves the compatibility between the comb-shaped PVP(PDP) block and the polyisoprene block to the extent that microphase separation does not occur for the short PVP blocks used (M_n of 1000 and 2800 g/mol). Short PVP block lengths are required because after hydrogen bonding to alkyl tail amphiphiles the thus-formed comb-shaped blocks should still be the minority component, accounting for less than ca. 30% of the material, to form cylinders. Hence, to increase the incompatibility between the PI-block and the PVP-based comb-shaped block, we subsequently selected octyl gallate (OG) (see Scheme 1) as the hydrogen-bonding amphiphile. Not only does OG have a shorter alkyl tail than PDP, but it is also far more polar due to the three hydroxyl groups and the ester group. In a different context, alkyl gallates have been used before to induce self-assembly in pyridine-containing polymers.[30−32]

As it turns out, the use of OG gives rise to very interesting phase behavior for the PI-*b*-P2VP-based systems. The use of OG does not lead to hierarchically ordered structures: the octyl tail is simply too short to induce additional microphase separation inside the PVP(OG) domains. However, since we are aiming at mesoporous materials by dissolving the amphiphiles after they have served their role in the self-assembly process, this is of no consequence here. All samples investigated are collected in Table 1.

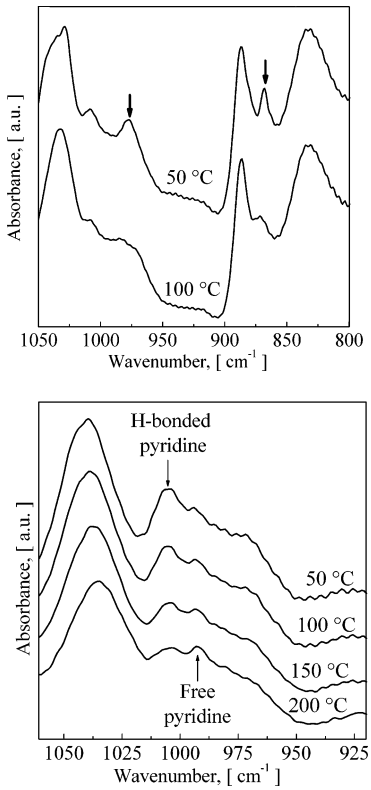

Figure 1. (a) FTIR spectra of PI-*b*-P2VP(OG)$_{1.20}$ at 50 and 100 °C showing the disappearance of the characteristic bands of crystallized OG (indicated with arrows) at about 978 and 868 cm^{-1}. (b) FTIR spectra of PI-*b*-P2VP(OG)$_{0.25}$ as a function of temperature demonstrating the gradual reduction in number of hydrogen bonds.

Pure octyl gallate is usually in the crystal form below ca. 95 °C as a dihydrate. It forms a typical bilayer head-to-head structure with interdigitated alkyl chains.[33] The gallate headgroups are hydrogen bonded through the three hydroxyls, the carbonyl group, and the two water molecules. DSC measurements show two endothermic peaks at 92.3 and 95.6 °C. The first peak is believed to be due to a crystal-to-crystal structure transition, possibly involving dehydration. The second peak is due to the melting. The melting of octyl gallate is also clearly visible in the infrared spectrum.

Our investigation of the PI-*b*-PVP(OG)$_x$ systems have shown that for large amounts of OG (i.e., $x \geq 1.0$) crystallization of octyl gallate also occurs in combination with the block copolymers studied. The presence and disappearance of crystalline OG in the samples involving a relatively large amount of OG are demonstrated by the FTIR data of PI-*b*-P2VP(OG)$_{1.2}$, presented in Figure 1a. At 50 °C two characteristic bands of crystalline OG at 870 and 970 cm^{-1} are observed, while they have disappeared at 100 °C.

Besides crystallization, another feature of OG is its ability to potentially make multiple hydrogen bonds, maybe even leading to a physically cross-linked network inside the PVP(OG) domain. However, rheological measurements involving P2VP or P4VP homopolymers together with octyl gallate did not reveal any sign of such physical cross-links, and hence, if present at all, they are probably of no consequence for the self-assembly. Before presenting the phase behavior of the PI-*b*-PVP(OG) systems, we will first briefly discuss the extent of hydrogen bonding between pyridine and OG as a function of temperature using infrared spectros-

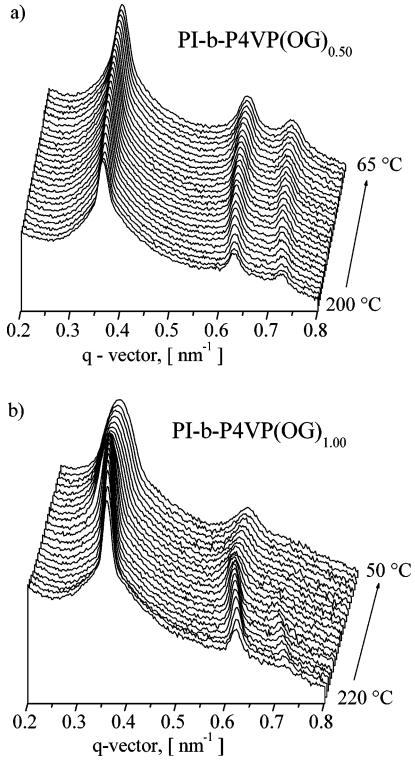

Figure 2. SAXS of (a) PI-*b*-P4VP(OG)$_{0.5}$ and (b) PI-*b*-P4VP(OG)$_{1.0}$ on cooling from 200/220 °C at 10 °C/min. Every frame was measured for 30 s.

copy. It is known that hydrogen-bonded pyridine gives rise to a broad band at 1005−1010 cm^{-1}, compared to 993 cm^{-1} band for the free pyridine ring.[30] Additionally, there is a shift of the 1036 cm^{-1} band of the free pyridine to the 1039 cm^{-1} band of hydrogen-bonded pyridine. The effect of temperature on the IR spectrum is shown in Figure 1b for PI-*b*-P2VP(OG)$_{0.25}$. This particular sample is selected because for a higher amount of OG the free pyridine ring band is not visible anymore due to overlapping with the OG molecule band. The FTIR data show that a considerable reduction in the number of hydrogen-bonded pyridine has already taken place at temperatures above 100 °C. At temperatures above 190 °C there is an almost complete absence of H-bonds.

PI-*b*-P4VP(OG) Systems. The pure block copolymer PI-*b*-P4VP and the PI-*b*-P4VP(OG)$_{0.25}$ system do not show any signs of self-assembly. Their SAXS patterns consist of only one broad and weak scattering peak, which, however, is slightly more prominent for the OG sample.

The PI-*b*-P4VP(OG)$_x$ samples with $x = 0.5$, 0.75, 1.0, and 1.2 all exhibit a hexagonally ordered cylindrical self-assembly, characterized by 1:$\sqrt{3}$:2 scattering peaks, throughout the experimental temperature range investigated. The SAXS patterns of the $x = 0.5$ and 1.0 samples are presented in Figure 2.

The values q^* of the scattering vector corresponding to the position of the first peak of these patterns are collected in Table 2. The data have been obtained at $T \cong 170$ °C, where the peaks were sharpest. With a knowledge of the characteristic cell geometry and the weight fraction of PI and P4VP(OG), we calculated the cylinder diameters assuming that weight fraction ≅ volume fraction, which is not too far from reality, and that all OG molecules are in the P4VP phase. As can be seen from the table, the role of the amount of octyl gallate in relation to the final cylinder diameter is

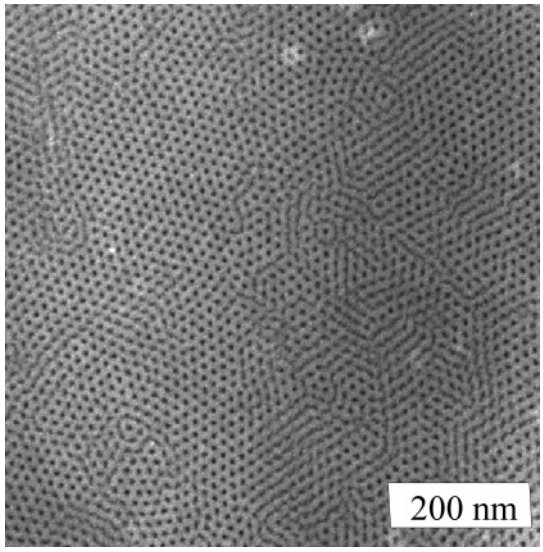

Figure 3. TEM image of the shear-aligned cylindrical morphology of P4VP(OG)$_{0.75}$ cylinders in a matrix of PI.

Table 2. Characteristic Properties of PI-*b*-P4VP(OG)$_x$ at 170 °C

sample	q^*, nm^{-1}	structure	4VP(OG)-cylinder diam, nm	empty cylinder diam, nm
PI-*b*-P4VP	0.424	disordered		
PI-*b*-P4VP(OG)$_{0.25}$	0.385	disordered		
PI-*b*-P4VP(OG)$_{0.50}$	0.358	cylindrical	8.5	4.5
PI-*b*-P4VP(OG)$_{0.75}$	0.355	cylindrical	9.4	5.9
PI-*b*-P4VP(OG)$_{1.00}$	0.351	cylindrical	10.4	7.2
PI-*b*-P4VP(OG)$_{1.20}$	0.341	cylindrical	11.2	8.2

obvious, and the data clearly demonstrate how octyl gallate can be used to tune the pore size. Assuming that after removal of OG the PVP blocks are collapsed onto the polyisoprene walls results in a diameter of the empty cylinders varying from 4.5 to 8.2 nm.

To image the hexagonally ordered cylindrical structure of PI-*b*-P4VP(OG)$_{0.75}$, the sample was macroscopically aligned by applying a large-amplitude oscillatory shear for 3 h at 90 °C with a frequency of 0.5 Hz and 100% strain. The good alignment achieved was confirmed by SAXS (not shown) and the electron microscopy picture shown in Figure 3.

The phase diagram of the PI-*b*-P4VP(OG)$_x$ systems is rather simple: no self-assembly occurs for the pure block copolymer and for $x = 0.25$, whereas only hexagonally ordered cylindrical structures are observed for higher amounts of OG. At first sight, the ubiquitous presence of cylindrical structures comes as no surprise given the fact that the weight fraction of the comb-shaped P4VP(OG)$_x$ blocks varies between 15.8% w/w for $x = 0.50$ to 25.2% w/w for $x = 1.20$. Ignoring the difference between weight and volume fraction, in the case of pure diblock copolymers this would put the composition indeed right inside the hexagonally ordered cylinders regime. However, as will be shown below, the situation is considerably more complex for the corresponding PI-*b*-P2VP-based samples, to which we will turn our attention next.

PI-*b*-P2VP(OG) Systems. At room temperature the SAXS patterns of the pure copolymer consists of two rather broad scattering peaks whose positions are in the ratio 1:$\sqrt{3}$ and can be assigned to a very poorly ordered cylindrical structure. On heating, the sample reveals a cubic structure at ca. 120 °C. This structure exists up

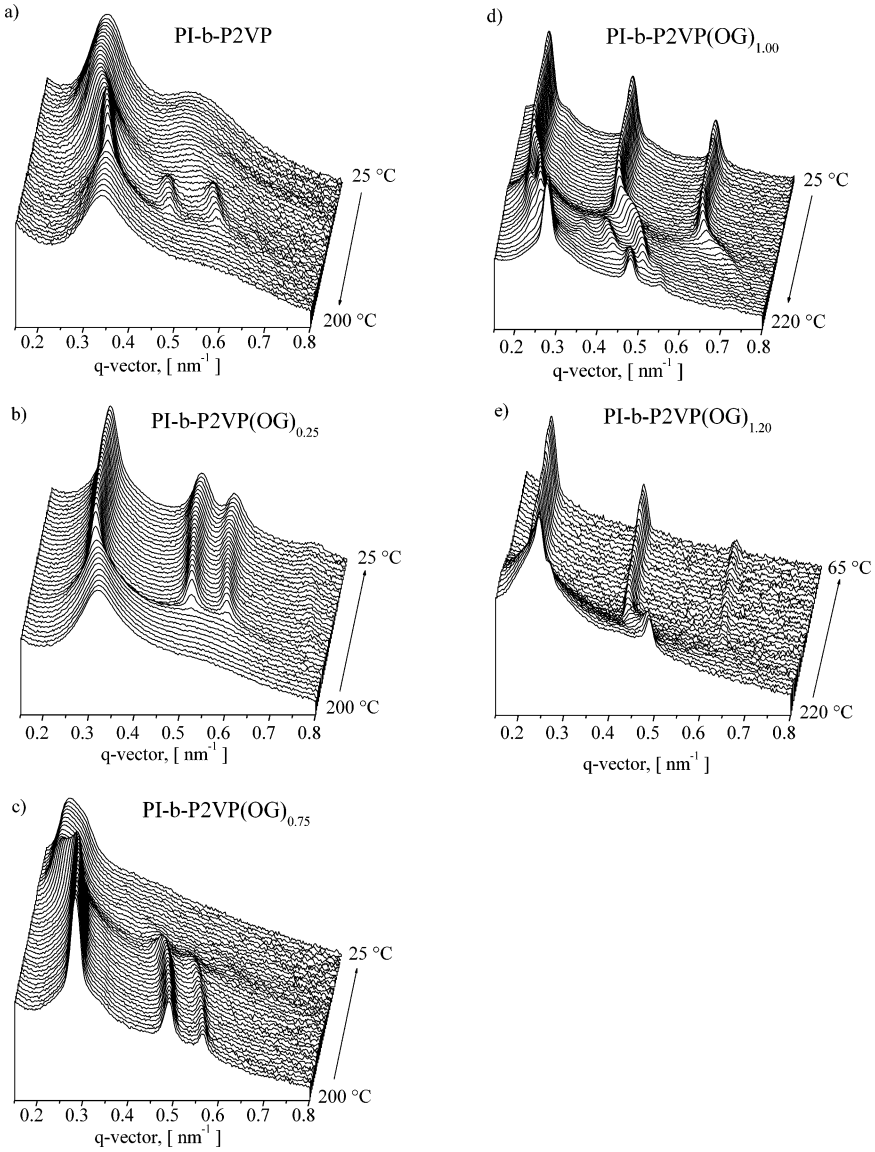

Figure 4. SAXS patterns of (a) PI-*b*-P2VP, (b) PI-*b*-P2VP(OG)$_{0.25}$, (c) PI-*b*-P2VP(OG)$_{0.75}$, (d) PI-*b*-P2VP(OG)$_{1.0}$, and (e) PI-*b*-P2VP(OG)$_{1.20}$, collected during heating or cooling at 10 °C/min. Arrows indicate temperature direction.

to 160 °C, where the sample undergoes an order−disorder transition. A series of SAXS patterns collected on heating to 200 °C are shown in Figure 4a. On cooling, the sample shows a reversible behavior going back to its original state. The existence of a hexagonal structure is rather surprising since the weight fraction of P2VP in the diblock copolymer is only 8.5%.

The PI-*b*-P2VP(OG)$_{0.25}$ and PI-*b*-P2VP(OG)$_{0.50}$ samples show SAXS peaks that are characteristic for cylindrical self-assembly. This is not unexpected since it corresponds to a weight fraction of the comb-shaped P2VP(OG) block of 11.8% and 15.8% w/w, respectively. On heating at 10 °C/min, PI-*b*-P2VP(OG)$_{0.25}$ undergoes an order−disorder transition at 190 °C, while on cooling with the same rate the sample goes back to the cylindrical structure at ca. 145 °C only. The SAXS patterns recorded during cooling of this sample are presented in Figure 4b. If the scanning rate is changed from 10 to 5 °C/min, this surprisingly large hysteresis effect is reduced to 20 °C (170 and 150 °C on heating and cooling, respectively). Hence, it seems to be related to the molecular mobility. However, it is of interest to note that, in contrast to this order−disorder transition, all the order−order transitions, to be discussed, do not exhibit similar strong hysteresis effects.

The SAXS patterns of PI-*b*-P2VP(OG)$_{0.50}$ are not shown here because they are essentially similar to the PI-*b*-P2VP(OG)$_{0.25}$ patterns apart from the absence of an order−disorder transition.

The PI-*b*-P2VP(OG)$_{0.75}$ sample also forms a cylindrical structure, but only at temperatures above 100 °C. The SAXS patterns of this sample obtained on cooling from 200 to 25 °C are presented in Figure 4c. An abrupt decrease in the first peak intensity at ca. 100 °C can be seen together with the disappearance of the higher order reflections of the cylindrical structure. Below this temperature, two structures are faintly observable: the cylindrical structure and a newly formed lamellar structure with the corresponding q^* peak having as a shoulder on the cylindrical phase peak. At these temperatures, the molecular mobility is considerably reduced, and the equilibration of the structure during the cooling at 10 °C/min is apparently strongly hampered. The transition to a lamellar structure is somewhat unexpected taking into account the weight fraction of 21.9% w/w for the P2VP(OG)$_{0.75}$ block. However, it is in

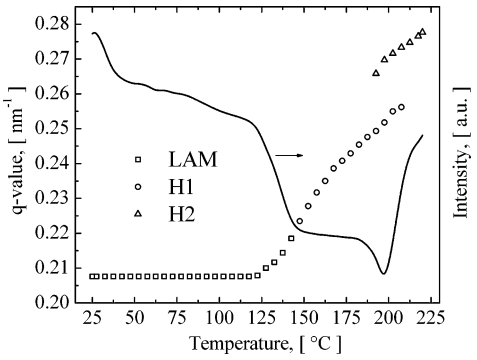

Figure 5. Position q^* and intensity $I(q^*)$ of the main scattering peak observed for the PI-*b*-P2VP(OG)$_{1.0}$ sample as a function of temperature.

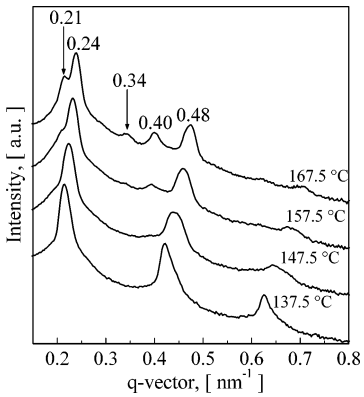

Figure 6. SAXS patterns of PI-*b*-P2VP(OG)$_{1.0}$ at indicated temperatures.

Table 3. Characteristic Properties of PI-*b*-P2VP(OG)$_x$ at 170 °C

sample	q^*, nm^{-1}	structure	2VP(OG)-cylinder *d*-spacing, nm	empty cylinder diam, nm
PI-*b*-P2VP(OG)$_{0.25}$	0.296	cylindrical	9.4	3.4
PI-*b*-P2VP(OG)$_{0.50}$	0.285	cylindrical	11.7	6.2
PI-*b*-P2VP(OG)$_{0.75}$	0.276	cylindrical	12.9	8.1

line with the observation that the comb-shaped nature of the P2VP(OG) block is expected to result in a preference for a less inward curved interface of the P2VP(OG) domains.[34]

The main scattering peak q^* values derived from the SAXS data of PI-*b*-P2VP(OG)$_x$, $x = 0.25$, 0.50, and 0.75, at a temperature of 170 °C, where all three consist of a hexagonally ordered cylindrical structure, are collected in Table 3. The corresponding cylinder diameters also presented in the table were calculated in the same way as described above.

The PI-*b*-P2VP(OG)$_{1.00}$ sample exhibited a far more complex phase behavior. SAXS patterns obtained during heating in the temperature interval of 25−220 °C are shown in Figure 4d. The sample has a lamellar structure up to ca. 150 °C. As shown in Figure 5, the q^* value of the first-order reflection of the lamellar structure, and thus the long period $d = 2\pi/q^*$, is quite insensitive to temperature up to 120 °C. This may be related to the supramolecular nature of the comb-shaped block, where the number of hydrogen bonds between P2VP and OG starts to decrease significantly only around this temperatures. The fact that OG is in a crystalline state below ca. 95 °C may play an important role as well.

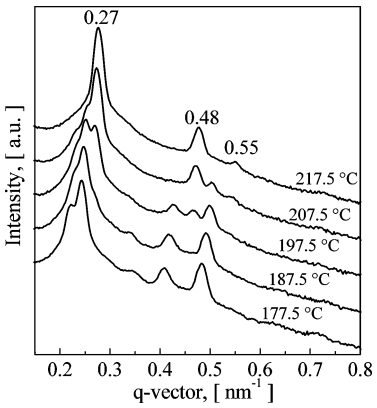

Figure 7. SAXS patterns of PI-*b*-P2VP(OG)$_{1.0}$ as a function of temperature.

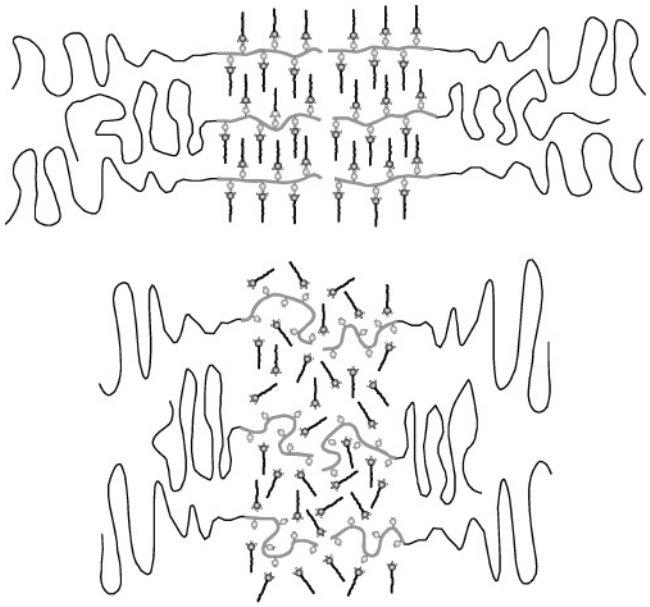

Figure 8. Illustration of reduction in characteristic length scale as a result of the relaxation of the P2VP blocks. The upper scheme describes the low-temperature stretched chains due to the hydrogen-bonded side chains, whereas the lower scheme describes the situation where the side chains are not hydrogen bonded to the backbones and are only miscible in the P2VP domains due to the polarity of both components, thus leading to a collapse of the periodicity.

The periodicity of the lamellar structure starts to decrease strongly above 120 °C. On further heating, at 150 °C an order−order transition toward a hexagonal structure takes place. A detailed picture of the corresponding change in the SAXS patterns is presented in Figure 6. Apart from the peaks of the hexagonal structure clearly observed at $q = 0.24$, 0.40, and 0.48 nm^{-1}, which will be referred to as H1, there are two additional peaks at 0.21 and 0.34 nm^{-1}, indicated by arrows in Figure 6. The latter might correspond to the lamellar to cylindrical phase transition mechanism as discussed by Hajduk et al.[35] In this view, the transformation of the lamellar structure starts with the formation of cylinders inside the lamellae followed by their packing into a hexagonal lattice. The peaks at 0.21 nm^{-1} and 0.34 nm^{-1} may originate from a deformed hexagonal structure of cylinders through which the system must pass on its way from lamellar to hexagonally packed cylinders. The characteristic *d* spacing between these cylinders may give rise to the 0.34 nm^{-1} peak (it corresponds to 18.47 nm). On further increasing the

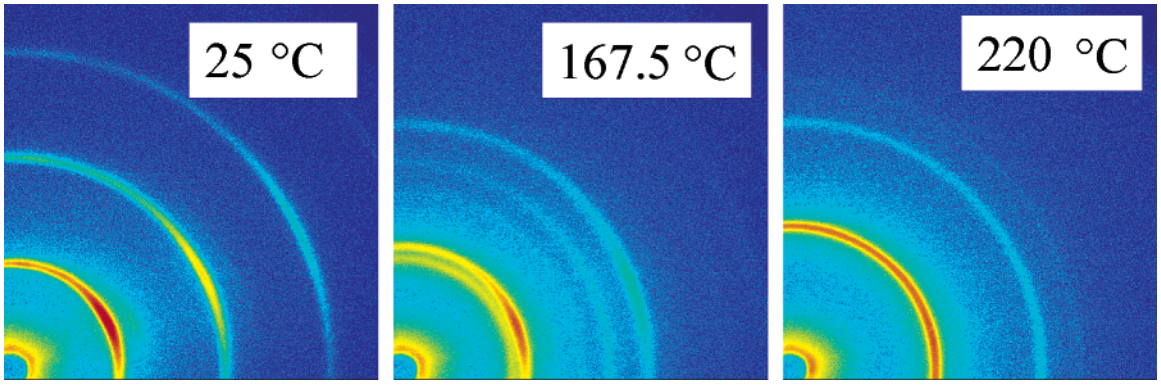

Figure 9. SAXS patterns of PI-*b*-P2VP(OG)$_{1.0}$: (a) lamellar at 25 °C, (b) intermediate structure at 167.5 °C, and (c) hexagonal H2 structure at 220 °C.

temperature, this H1 structure exists only up to 190 °C, where a new transformation starts, as illustrated by the detailed SAXS patterns presented in Figure 7. This second transformation ends with a pure cylindrical structure, which will be referred to as H2. Its formation is accompanied by the appearance of very intensive new scattering peaks at larger q values. We believe that the increase in q value is related to the disappearance of almost all hydrogen bonds. As long as a substantial number of side chains are hydrogen bonded to the backbone, the P2VP backbone is in a strongly stretched conformation.[36] The reduction in hydrogen bonds allows the P2VP chains to relax from their strongly stretched conformation, resulting in a reduced characteristic length scale. At these temperatures OG is still insoluble in the PI phase, so we may assume that the cylinders inside the PI matrix consists of a mixture of P2VP and OG molecules, no longer forming comb-shaped hydrogen-bonded blocks. The cartoon, Figure 8, illustrates this. The transformation is complete at 210 °C. Heating was continued up to 220 °C, during which no further changes were observed. All phase transitions happened to be reversible. In Figure 9 the characteristic 2-dimensional scattering patterns of the PI-*b*-P2VP(OG)$_{1.00}$ sample, corresponding to its three different structures, are shown. The pattern of Figure 9a obtained at room temperature corresponds to the lamellar structure. As the sample undergoes some shearing upon inserting into the Linkam heating cell, the lamellar structure is somewhat aligned, leading to a slightly anisotropic pattern. The epitaxial growth of the H1 structure from the lamellar structure on heating is confirmed by the anisotropic SAXS pattern presented in Figure 9b. During the transition to the H2 structure, a considerable change in the d spacing occurs, and the original anisotropy is completely destroyed. The corresponding isotropic SAXS pattern is shown in Figure 9c.

Finally, we consider the behavior of the PI-*b*-P2VP(OG)$_{1.20}$ sample. The SAXS patterns recorded during cooling are shown in Figure 4e. It is evident that the sample has a lamellar structure (LAM1) at room temperature. This structure is present up to 190 °C. Above this temperature two more peaks are present, corresponding to a second lamellar structure (LAM2). A detailed picture of the SAXS patterns during this transition can be seen in Figure 10. Again, this phase transformation can be attributed to an almost complete breaking of H-bonds between the OG molecules and P2VP at high temperatures. The formation of hydrogen bonds on cooling leads to P2VP chain stretching and a corresponding expansion of the lamellar thickness.

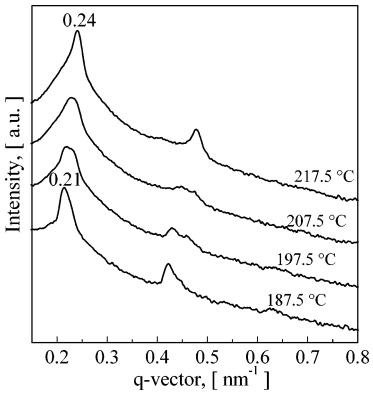

Figure 10. SAXS patterns of PI-*b*-P2VP(OG)$_{1.2}$ collected during heating at indicated temperatures.

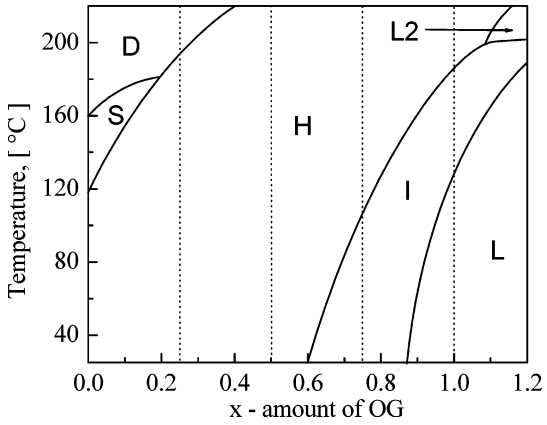

Figure 11. Qualitative phase diagram of PI-*b*-P2VP(OG)$_x$ as a function of the amount of octyl gallate x plotted according to the SAXS observations for $x = 0$, 0.25, 0.50, 0.75, 1.0, and 1.2. D, S, H, L, L2 denote disordered, spherical, hexagonal, lamellar, and lamellar structure with reduced spacing. I indicates intermediate state corresponding to a transistion usually involving the presence of two different structures.

On the basis of all the SAXS data, we constructed a qualitative "phase diagram" (Figure 11) for the PI-*b*-P2VP(OG)$_x$ system. The dashed lines and the solid borderlines at $x = 0$ and $x = 1.2$ correspond to the actual compositions investigated. The different phase transitions of these systems have been thoroughly described in the previous pages. The phase boundary lines smoothly connect in the (x, T) plane the transition temperatures observed at fixed values of x.

Concluding Remarks

In comparison to the 1,2-PI-*b*-P4VP(OG) systems, the phase behavior of the 1,4-PI-*b*-P2VP(OG) systems ap-

pears to be very rich and considerably more complex, as demonstrated by the SAXS data presented. This must somehow be related to the fact that the P4VP blocks are very short, only 10 monomers on average, compared to the P2VP blocks containing ca. 28 monomers. The most important ingredient of our explanation of the complex phase behavior of the PI-*b*-P2VP(OG) systems is the P2VP chain conformation "shrinkage" that occurs on heating due to the disappearance of the hydrogen-bonded side chains. Apparently, the P4VP blocks are too short for such arguments to hold.

Most of the comb-shaped supramolecules systems studied by us have a substantial mobility in common. After all, at elevated temperatures many of the hydrogen bonds are broken, and the amphiphiles act merely as a selective solvent. Consequently, it is not always easy to arrest the high-temperature structures to obtain reliable electron microscopy data. In the present case this is particularly true due to the involvement of polyisoprene rather than polystyrene blocks. Still, we hope to address these structures by electron microscopy in a future publication, since the SAXS data alone are not sufficient to determine the exact structures during the various order−order transitions.

Another aspect concerns their behavior under large-amplitude oscillatory shear. Recent experiments on the 1,4-PIp-*b*-P2VP(OG) systems demonstrate an essentially different behavior under shear compared to quiescent conditions. This difference appears to be due to the breakage of hydrogen bonds under shear. A full discussion for a few selected systems will be presented elsewhere.[37]

References and Notes

(1) Hamley, I. W. *The Physics of Block Copolymers*; Oxford University Press: New York, 1998.
(2) Bates, F. S.; Fredrickson, G. H. *Annu. Rev. Phys. Chem.* **1990**, *41*, 525.
(3) Muthukumar, M.; Ober, C. K.; Thomas, E. L. *Science* **1999**, *277*, 1225.
(4) Chen, J. T.; Thomas, E. L.; Ober, C. K.; Mao, G.-P. *Science* **1996**, *273*, 343.
(5) Bates, F. S.; Fredrickson, G. H. *Phys. Today* **1999**, *52*, 32.
(6) Park, C.; Yoon, J.; Thomas, E. L. *Polymer* **2003**, *44*, 6725.
(7) Nanosciences; Special Issue of *Sci. Am.* **2001**, *285* (3).
(8) Faul, C. F. J.; Antonietti, M. *Adv. Mater.* **2003**, *15*, 673.
(9) Thünemann, A. F. *Prog. Polym. Sci.* **2002**, *27*, 1473.
(10) Ikkala, O.; ten Brinke, G. *Science* **2002**, *295*, 2407.
(11) Ruokolainen, J.; Mäkinen, R.; Torkkeli, M.; Mäkelä, T.; Serimaa, R.; ten Brinke, G.; Ikkala, O. *Science* **1998**, *280*, 557.
(12) Ruokolainen, J.; Saariaho, M.; Ikkala, O.; ten Brinke, G.; Thomas, E. L.; Torkkeli, M.; Serimaa, R. *Macromolecules* **1999**, *32*, 1152.
(13) Ruokolainen, J.; ten Brinke, G.; Ikkala, O. *Adv. Mater.* **1999**, *11*, 777.
(14) Valkama, S.; Lehtonen, O.; Lappalainen, K.; Kosonen, H.; Castro, P.; Repo, T.; Torkkeli, M.; Serimaa, R.; ten Brinke, G.; Leskelä, M.; Ikkala, O. *Macromol. Rapid Commun.* **2003**, *24*, 556.
(15) Ruokolainen, J.; Tanner, J.; ten Brinke, G.; Ikkala, O.; Torkkeli, M.; Serimaa, R. *Macromolecules* **1995**, *28*, 7779.
(16) Kato, T.; Frechet, J. M. J. *Macromolecules* **1989**, *22*, 3818.
(17) Navarro-Rodriquez, D.; Guillon, D.; Skoulios, A. *Makromol. Chem.* **1992**, *193*, 3117.
(18) Kato, T.; Kihara, H.; Ujiie, S.; Uryu, T.; Frechet, J. M. J. *Macromolecules* **1996**, *29*, 8734.
(19) Brandys, F. A.; Bazuin, C. G. *Chem. Mater.* **1996**, *8*, 83.
(20) Kato, K. *Macromol. Rapid Commun.* **2001**, *22*, 797.
(21) Kato, T. *Science* **2002**, *295*, 2414.
(22) Ruokolainen, J.; Torkkeli, M.; Serimaa, R.; Komanschek, B. E.; Ikkala, O.; ten Brinke, G. *Phys. Rev. E* **1996**, *54*, 6646.
(23) Mäkinen, R.; de Moel, K.; de Odorico, W.; Ruokolainen, J.; Stamm, M.; ten Brinke, G.; Ikkala, O. *Adv. Mater.* **2001**, *13*, 107.
(24) Mäkinen, R.; Ruokolainen, J.; Ikkala, O.; de Moel, K.; ten Brinke, G.; de Odorico, W.; Stamm, M. *Macromolecules* **2000**, *33*, 3441.
(25) de Moel, K.; Mäkinen, R.; Stamm, M.; Ikkala, O.; ten Brinke, G. *Macromolecules* **2001**, *34*, 2892.
(26) Polushkin, E.; Alberda van Ekenstein, G. O. R.; Dolbnya, I.; Bras, W.; Ikkala, O.; ten Brinke, G. *Macromolecules* **2003**, *36*, 1421.
(27) Alberda van Ekenstein, G. O. R.; Polushkin, E.; Nijland, H.; Ikkala, O.; ten Brinke, G. *Macromolecules* **2003**, *36*, 3684.
(28) Kim, S. H.; Misner, M. J.; Xu, T.; Kimura, M.; Russell, T. P. *Adv. Mater.* **2004**, *16*, 226.
(29) Sidorenko, A.; Tokarev, I.; Minko, S.; Stamm, M. *J. Am. Chem. Soc.* **2003**, *125*, 12211.
(30) Ruokolainen, J.; Torkkeli, M.; Serimaa, R.; Vahvaselkä, S.; Saariaho, M.; ten Brinke, G.; Ikkala, O. *Macromolecules* **1996**, *29*, 6621.
(31) Ikkala, O.; Knaapila, M.; Ruokolainen, J.; Torkkeli, M.; Serimaa, R.; Jokela, K.; Horsburgh, L.; Monkman, A. P.; ten Brinke, G. *Adv. Mater.* **1999**, *11*, 1206.
(32) Knaapila, M.; Stepanyan, R.; Horsburgh, L. E.; Monkman, A. P.; Serimaa, R.; Ikkala, O.; Subbotin, A.; Torkkeli, M.; ten Brinke, G. *J. Phys. Chem. B* **2003**, *107*, 14199.
(33) Jeffrey, G. A.; Yeon, Y. *Acta Crystallogr.* **1990**, *B46*, 519.
(34) Milner, S. T. *Macromolecules* **1994**, *27*, 2333.
(35) Hajduk, D. A.; Gruner, S. M.; Rangarajan, P.; Register, R. A.; Fetters, L. J.; Honeker, C.; Albalak, R. J.; Thomas, E. L. *Macromolecules* **1994**, *27*, 490.
(36) V. V. Vasilevskaya, V. V.; Gusev, L. A.; Khokhlov, A. R.; Ikkala, O.; ten Brinke, G. *Macromolecules* **2001**, *34*, 5019.
(37) Polushkin, E.; Bondzic, S.; ten Brinke, G.; Bras, W.; Dolbnya, I.; Ikkala, O., to be published.

MA048913R